

Metasurface covered millimeter-wave MIMO antenna array

Mohammad Alibakhshikenari , Iftikhar ud Din , Esraa Mousa Ali , Nouf Abd Elmunim , Bal S. Virdee , Dion Mariyanayagam , Sadiq Ullah , Nisar Ahmad Abbasi , Nasr Rashid , Chan Hwang See , Takfarinas Saber , Francisco Falcone & Ernesto Limiti

To cite this article: Mohammad Alibakhshikenari , Iftikhar ud Din , Esraa Mousa Ali , Nouf Abd Elmunim , Bal S. Virdee , Dion Mariyanayagam , Sadiq Ullah , Nisar Ahmad Abbasi , Nasr Rashid , Chan Hwang See , Takfarinas Saber , Francisco Falcone & Ernesto Limiti (23 Oct 2025): Metasurface covered millimeter-wave MIMO antenna array, Waves in Random and Complex Media, DOI: [10.1080/17455030.2025.2574631](https://doi.org/10.1080/17455030.2025.2574631)

To link to this article: <https://doi.org/10.1080/17455030.2025.2574631>



© 2025 The Author(s). Published by Informa UK Limited, trading as Taylor & Francis Group.



Published online: 23 Oct 2025.



[Submit your article to this journal](#)



Article views: 345



[View related articles](#)



[View Crossmark data](#)

Metasurface covered millimeter-wave MIMO antenna array

Mohammad Alibakhshikenari^{a,b}, Iftikhar ud Din^c, Esraa Mousa Ali^d, Nouf Abd Elmunim^e, Bal S. Virdee^f, Dion Mariyanayagam^f, Sadiq Ullah^c, Nisar Ahmad Abbasi^g, Nasr Rashid^{h,i}, Chan Hwang See^j, Takfarinas Saber^a, Francisco Falcone^k and Ernesto Limiti^l

^aLERO, the Research Ireland Centre for Software, College of Science and Engineering, School of Computer Science, University of Galway, Galway, Ireland; ^bDepartment of Electrical and Electronics Engineering, Dogus University, Istanbul, Turkey; ^cTelecommunication Engineering Department, University of Engineering and Technology, Mardan, Pakistan; ^dCommunications and Computer Engineering Department, Al-Ahliyya Amman University, Amman, Jordan; ^eDepartment of Electrical Engineering, College of Engineering, Princess Nourah bint Abdulrahman University, Riyadh, Saudi Arabia; ^fCenter for Communications Technology, London Metropolitan University, London, UK; ^gDepartment of Electrical Engineering, School of Systems Engineering, Bahrain Polytechnic, Isa Town, Bahrain; ^hElectrical Engineering Department, College of Engineering, Jouf University, Sakaka, Saudi Arabia; ⁱDepartment of Electrical Engineering, Faculty of Engineering, Al-Azhar University, Nasr City, Cairo, Egypt; ^jSchool of Engineering and the Built Environment, Edinburgh Napier University, Edinburgh, UK; ^kInstitute of Smart Cities, Department of Electric, Electronic and Communication Engineering, Public University of Navarre, Pamplona, Spain; ^lElectronics Engineering Department, University of Rome "Tor Vergata", Rome, Italy

ABSTRACT

This paper describes the design of a unique 26 GHz Multiple-Input, Multiple-Output (MIMO) antenna array for 5G millimeter-wave (mm-Wave) broadband applications. The antenna comprises a 2×1 array of radiating elements excited through a T-junction power divider. The antenna array, with dimensions of $12 \times 18 \text{ mm}^2$, offers a wide operational bandwidth between 25.05 and 27.8 GHz, corresponding to a fractional bandwidth of 10.4%. It is a modified four-element MIMO system, in which the radiating elements are arranged in parallel with an inter-element spacing of $1.5\lambda_0$ at 26 GHz and oriented orthogonally to one another. To further enhance the gain, isolation, and overall performance, a metasurface layer comprising a 5×6 array of rectangular split-ring resonators (RSRs) is strategically placed above the antenna. This metasurface acts as a passive spatial filter and phase modulator, enabling wavefront shaping and polarization control. Constructed on a Rogers RT/duroid substrate with a thickness of 0.8 mm, the proposed MIMO system achieves an average gain of 7.85 dBi, a peak gain of 9.1 dBi at 25.8 GHz, an inter-element isolation of -24 dB , and an ECC of less than 0.0005.

ARTICLE HISTORY

Received 7 July 2024
Accepted 6 October 2025

KEYWORDS




Multiple-input multiple-output (MIMO); antenna array; metasurface; 5G millimeter-wave (mm-Wave); T-junction power divider

1. Introduction

In the modern era, the explosive growth of wireless devices has driven a transformative shift in mobile communications [1–3]. This evolution is marked by an annual data rate increase of 40–70%, and the demand for wireless communication has resulted in bandwidth requirements nearly 1000 times greater than those of previous-generation systems [4,5]. To meet these demands, fifth generation (5G) wireless technology has emerged as a powerful solution, offering data rates up to 20 Gbps and ultra-low latency as low as 1 ms [6,7].

However, the increasing need for higher data throughput and broader bandwidth is expected to render the 5G sub-6GHz spectrum insufficient. As a result, the adoption of the millimeter-wave (mmWave) spectrum has become essential [8]. The mmWave band offers significantly wider bandwidth, enabling gigabit wireless services. Additionally, it allows for the implementation of compact antenna structures, facilitating the integration of multiple antenna elements into a small form factor. This enables high gain and beamforming capabilities, even in mobile devices.

Recognizing the importance of mmWave technology, the Federal Communications Commission (FCC) has allocated several frequency bands for 5G deployment, including 24, 28, 37, 39, and 47 GHz. Extensive research has investigated the use of both sub-6 GHz (3–6 GHz) and mmWave (20–40 GHz) bands for 5G applications

CONTACT Mohammad Alibakhshikenari  mohammad.alibakhshikenari@universityofgalway.ie; Nouf Abd Elmunim  naasmil@pnu.edu.sa; Francisco Falcone  francisco.falcone@unavarra.es

© 2025 The Author(s). Published by Informa UK Limited, trading as Taylor & Francis Group.
This is an Open Access article distributed under the terms of the Creative Commons Attribution-NonCommercial-NoDerivatives License (<http://creativecommons.org/licenses/by-nc-nd/4.0/>), which permits non-commercial re-use, distribution, and reproduction in any medium, provided the original work is properly cited, and is not altered, transformed, or built upon in any way. The terms on which this article has been published allow the posting of the Accepted Manuscript in a repository by the author(s) or with their consent.

[9–13]. While mmWave bands offer high capacity, they also introduce challenges such as increased free-space path loss, atmospheric absorption, and signal degradation [14]. Therefore, achieving high gain at mmWave frequencies often requires deploying antenna arrays with multiple radiating elements.

To address these challenges while maintaining compactness, a variety of antenna structures have been explored. These include metamaterial-based antennas, Fabry–Perot cavities, and lens-coupled arrays [15–17]. Among these, MIMO (Multiple Input Multiple Output) systems play a vital role in 5G base stations by improving link reliability and boosting channel capacity with Gbps throughput [18,19]. However, compact MIMO designs must also mitigate mutual coupling, which can degrade overall system performance [20–22].

For instance, a 2×2 stacked patch MIMO antenna array was introduced in [23] for mmWave 5G base stations. Each element employed dual orthogonal stacked vias for circular polarization and achieved a peak gain of 6.5 dBi with mutual coupling below -20 dB. In recent years, metamaterials have gained traction for their unique electromagnetic properties and ability to improve antenna performance [24]. Several studies have demonstrated the benefits of metamaterial-enhanced MIMO antennas for mmWave applications [25–27]. For example: In [25], a bowtie-shaped MIMO array ($30.5 \times 30 \text{ mm}^2$) achieved a gain of 7.4 dBi over 24.25–27.7 GHz. In [26], an EBG structure improved the gain from 1.9 dBi to 6 dBi over a 1 GHz bandwidth ($27.5 \times 27.5 \text{ mm}^2$). In [27], a four-element DRA array achieved 7 dBi between 26.71 and 28.91 GHz using a metamaterial superstrate. In [28], a metasurface reflector boosted the gain of a two-element MIMO system to 11.5 dBi ($31.7 \times 53 \text{ mm}^2$). A compact two-port MIMO system in [29] reached 8.6 dBi from 29.7 to 31.5 GHz within a $48 \times 21 \text{ mm}^2$ footprint.

This paper proposes a 2×2 MIMO antenna array designed for 5G mmWave applications, offering high gain and compact size. The radiating elements are arranged orthogonally to enable circular polarization. A key innovation in this design is the integration of a metasurface layer, strategically positioned in front of the array. The metasurface shapes the phase of incident waves to produce constructive interference in the desired direction, effectively focusing radiated energy and increasing gain. This approach enhances the directivity and performance of the antenna system, while maintaining a simple, manufacturable design.

To overcome the limitations of conventional MIMO arrays at millimeter-wave frequencies, this work integrates a metasurface layer into the antenna architecture from the outset of the design process. The metasurface serves a dual role: first, as a spatial phase modulator that enhances directivity through constructive interference; and second, as a polarization filter that suppresses cross-polarized components, thereby improving gain and reducing coupling. Introducing this metasurface early in the design enables a more compact, high-performance antenna system suitable for 5G applications.

2. Antenna structure

The proposed MIMO system, as illustrated in Figure 1, comprises four radiating elements oriented orthogonally. These elements are constructed on a low-loss, high-frequency substrate made of Rogers RT/duroid 5880 with a dielectric constant (ϵ_r) of 2.2 and a substrate thickness (h) of 0.8 mm. Positioned in front of the array is a metasurface layer featuring a grid of 5×6 rectangular split-ring (RSR) resonators. Maintaining a 10 mm gap between the metasurface layer and the array is crucial for achieving the required radiation directivity.

To analyze and optimize the performance of the antenna array, we utilized CST Studio Suite, a 3D electromagnetic solver developed by Dassault Systèmes. Figure 1 provides a visual representation of the evolution of the radiating elements and, consequently, the antenna array. For a more comprehensive understanding of the antenna, a detailed explanation follows.

2.1. Antenna geometry

The proposed radiating element is derived from an edge-fed circular patch with a ground plane. The radius of the circular patch was determined using Equation (1) [30,31]. To enhance impedance matching between the feedline and the radiating element, a rectangular slot was introduced in the ground plane just below the patch antenna, as shown in Figure 2(a). Additionally, the width of the microstrip feed line was narrowed at the neck of the patch. This reduction in feed line width serves to lower the effective dielectric constant between the microstrip feed line and the ground plane. This alteration influences the effective electrical length of the feed line, aiding in the tuning process to achieve improved impedance matching. A rectangular slot in the ground plane was also employed to enhance the impedance matching and bandwidth characteristics of the antenna,

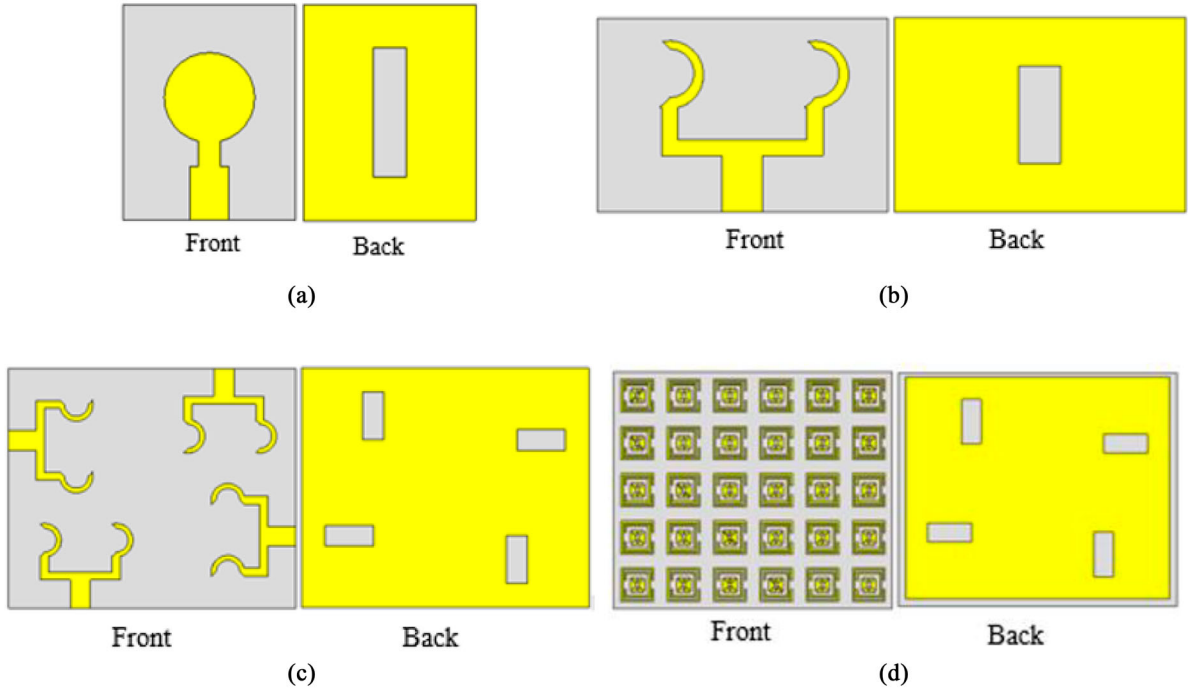


Figure 1. Evolution of aperture coupled antenna array, (a) Single disk-shaped radiating element, (b) Truncated radiating element in a 1×2 antenna array, (c) Configuration of the 2×2 antenna array, and (d) Metasurface cover.

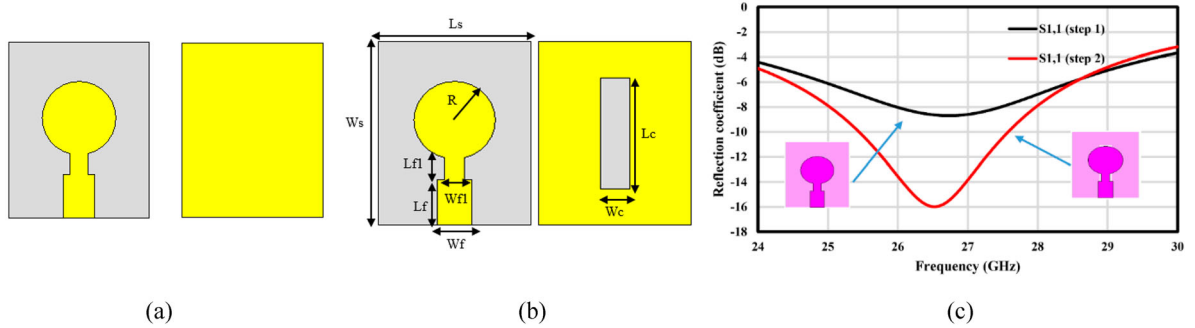


Figure 2. (a) Original disk-shaped optimized antenna, (b) With defected ground-plane, and (c) Reflection coefficient response of the optimized antenna and with defected ground-plane.

as shown in Figure 2(c). It's important to note that the size, shape, and position of the slot significantly affects the radiation characteristics and impedance bandwidth. Thus, careful design and optimization are imperative to attain the desired performance. The dimensions of the antenna structure are given in Table 1.

$$R = \frac{F}{\left\{ \sqrt{1 + \frac{2h}{\pi \epsilon_r F} (\ln \frac{\pi F}{2h} + 1.7726)} \right\}} \quad (1)$$

where

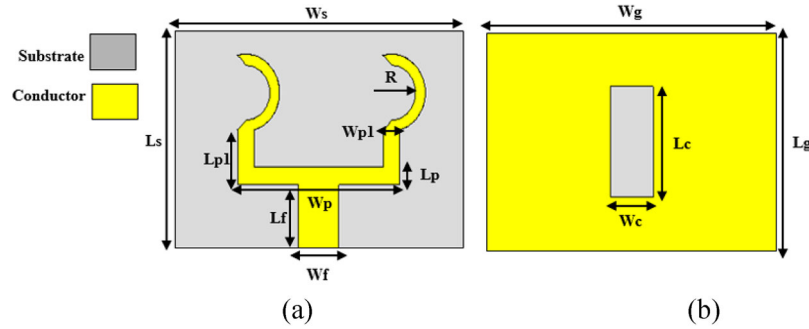
$$F = \frac{8.79 \times 10^9}{f_r \sqrt{\epsilon_r}}$$

2.2. Antenna array optimization

To improve the circular patch's reflection coefficient performance, it was transformed to a sickle shaped patch. The sickle shaped 2×1 array, shown in Figure 3, is excited through a T-junction power divider. The antenna

Table 1. Dimensions of the circular patch antenna.

| Parameter | Values (mm) | Parameter | Values (mm) |
|-----------|-------------|-----------|-------------|
| Wf | 1.8 | Wf1 | 1 |
| Lf | 2.5 | Lc | 6 |
| Lf1 | 1.7 | Wc | 1.6 |
| R | 2.1 | Ls | 10 |
| Ws | 8 | | |

**Figure 3.** The proposed 2×1 antenna array, (a) Top view, and (b) Bottom view.**Table 2.** Physical dimensions of the 2×1 MIMO antenna array.

| Parameter | Values (mm) | Parameter | Values (mm) |
|-----------|-------------|-----------|-------------|
| Wf | 2.3 | Ws | 17 |
| Lf | 3.0 | Wg | 17 |
| Wp1 | 1.15 | Lp | 2 |
| Lp1 | 1.15 | Wp | 8.57 |
| Ls | 17 | Wc | 2.3 |
| R | 2.3 | Lc | 7.4 |

array was constructed on Rogers RT/duroid 5880, a high frequency substrate with a rectangular slot implemented in the ground plane. The rectangular slot is used here to fine-tune the impedance matching to the antenna. By adjusting the size and position of the slot, the input impedance of the antenna can be controlled, which is essential for maximizing power transfer from the feedline to the antenna. The dimensions of the optimized antenna are given in Table 2.

The evolution of the 2×1 antenna array is depicted in Figure 4(a). The final antenna geometry is based on a standard circular patch antenna. Figure 4(b) illustrates how different modifications influenced the reflection coefficient (S_{11}). Initially, the impedance bandwidth for $S_{11} \leq -10$ dB is 3.2 GHz, ranging from 25.8 GHz to 29 GHz. By adding a rectangular slot to the ground plane, this bandwidth narrows to 1.5 GHz (from 23.3 GHz to 24.8 GHz) and 1.4 GHz (from 27 GHz to 28.4 GHz). Subsequently, converting the circular disk to a circular ring expands the impedance bandwidth to 3.3 GHz, spanning from 25.7 GHz to 29 GHz. Further transformation to a semi-circular ring enhances the reflection coefficient to -33 dB at 26.1 GHz and increases the impedance bandwidth to 2.8 GHz (from 25.1 GHz to 27.9 GHz).

2.3. MIMO based on linear arrangement of four radiating elements

The proposed 2×1 antenna array was utilized in the development of an 8×1 MIMO system. This configuration involved arranging the 2×1 antenna arrays in a linear format, as illustrated in Figure 5. The gap between neighboring 2×1 arrays is 18 mm (equivalent to $1.55\lambda_0$) at 26 GHz. The overall size of the 8×1 MIMO system is 12×72 mm².

This spacing was determined through parametric optimization using CST Studio Suite. A range of inter-element distances was simulated to evaluate trade-offs between mutual coupling, array footprint, and impedance performance. It was observed that $1.5\lambda_0$ provided the best compromise, which achieved low mutual coupling and envelope correlation while avoiding unnecessary enlargement of the array. Further

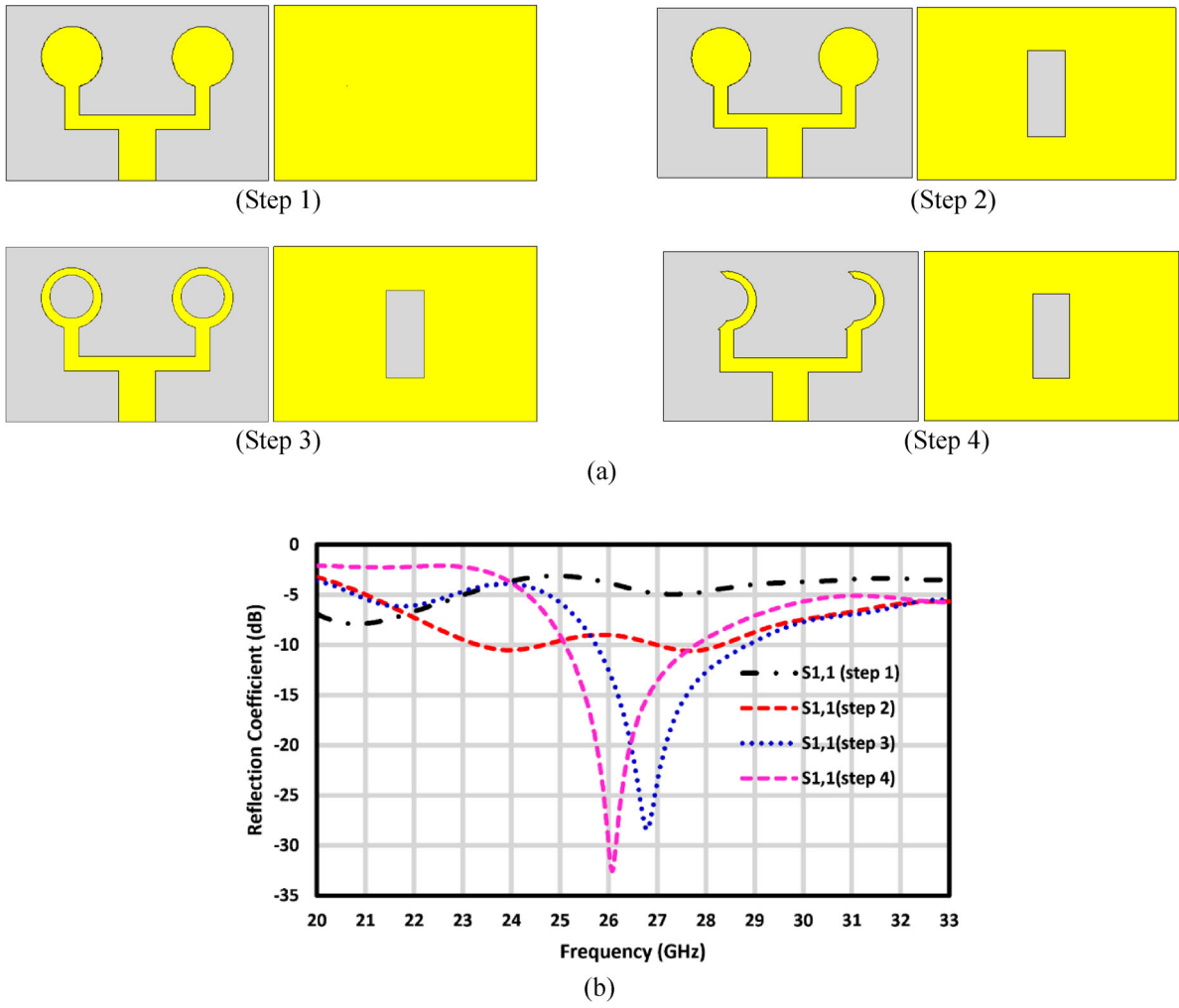


Figure 4. 2×1 Antenna array, (a) optimization steps, and (b) reflection coefficient responses.

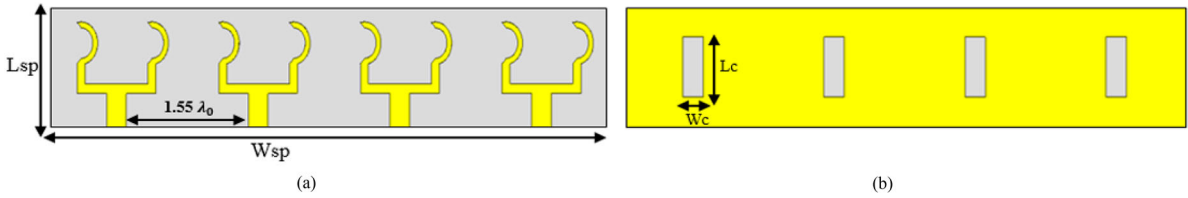


Figure 5. Linear arrangement of four 2×1 antenna arrays, (a) Front view, and (b) Back view.

increases in spacing yielded diminishing performance returns, while smaller gaps led to significantly higher coupling. Hence, $1.5\lambda_0$ was adopted as the optimal spacing based on simulation-driven empirical results.

The S-parameters for both the single element radiator and the four radiators arranged linearly are displayed in Figure 6. The single element antenna maintains a reflection coefficient of better than -10 dB across a 2.75 GHz bandwidth, spanning from 25.05 GHz to 27.8 GHz. The individual 2×1 antenna arrays, when arranged in parallel, exhibit an identical reflection coefficient response of -28 dB at 26 GHz, and the inter-element isolation or mutual coupling is higher than 32 dB.

2.4. MIMO based on orthogonal arrangement of four radiating elements

Investigation was done by arranging the four 2×1 antenna arrays orthogonally relative to each other, as illustrated in Figure 7. The ground plane is defected with rectangular slots that are located under each array. Figure

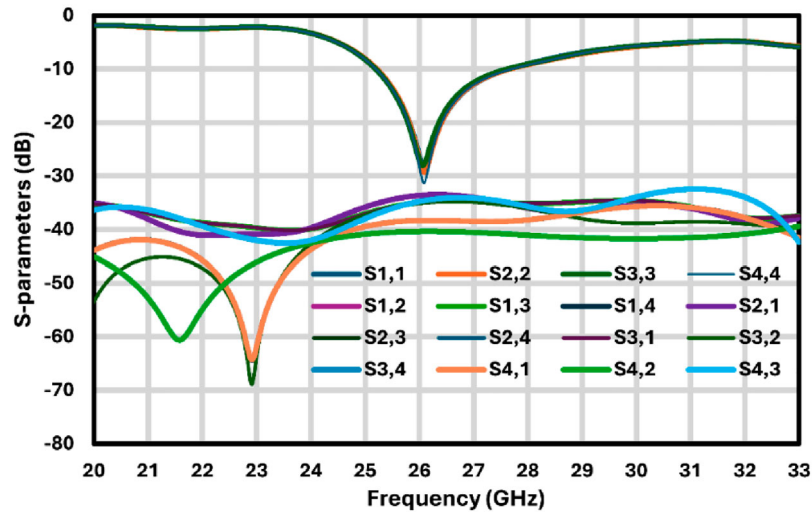


Figure 6. S-parameters a single element and four 2×1 antenna array MIMO system.

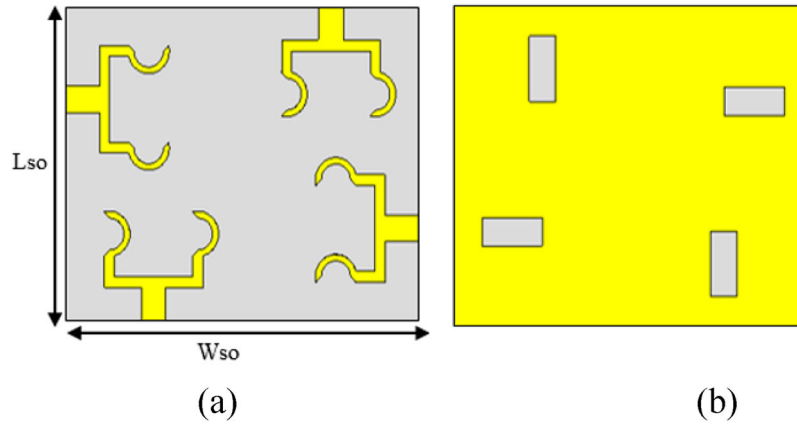


Figure 7. Orthogonally arranged four element 2×2 antenna array MIMO system, (a) Front view, and (b) Back view.

8 shows that the individual 2×1 antenna arrays in the orthogonal orientation exhibit an identical reflection coefficient response of -48 dB at 26.3 GHz, and the inter-element isolation or mutual coupling is higher than 25 dB.

The designation modified four-element MIMO system refers to structural enhancements introduced over conventional MIMO designs. Specifically, the radiating elements are oriented orthogonally to leverage polarization diversity and inherently reduce mutual coupling. Additionally, the inter-element spacing is set to $1.5\lambda_0$ at 26 GHz, an optimized compromise between minimizing near-field coupling and maintaining array compactness. These geometric modifications, combined with the use of a metasurface and defected ground structure (detailed in subsequent sections), form the basis of the array's enhanced electromagnetic behavior.

2.5. Metasurface unit cell

The metasurface is based on a square split-ring resonator. The metamaterial characteristic of negative refractive index is obtained by locating a slightly smaller split-ring inside another with the open ends facing opposite sides, as shown in Figure 9. Split-ring resonators are designed to resonate at certain frequencies when exposed to electromagnetic waves. When one split-ring resonator is placed inside another, their electromagnetic fields interact with each other in such a way to create a negative refractive index response. The interaction between the two SRRs leads to a phase delay in the electromagnetic wave passing through the material. The phase delay determines how the electromagnetic wave propagates through the material. When the phase delay is such that the wavefronts are bent in a particular way, it can lead to negative refraction. Negative refraction means

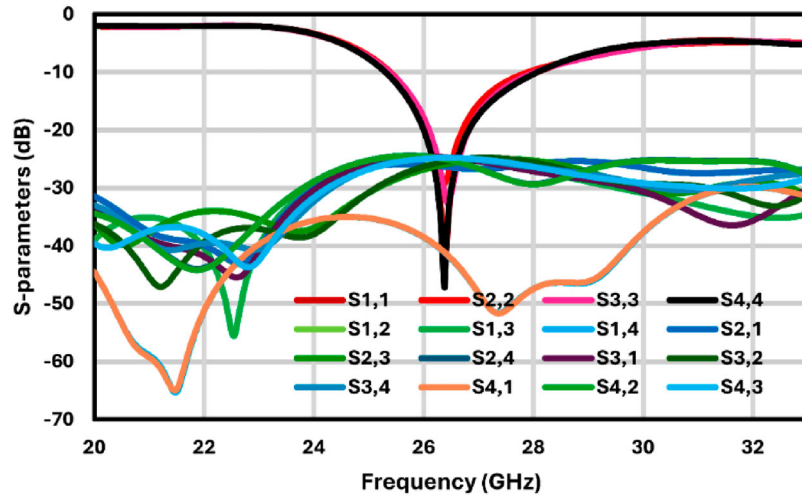


Figure 8. S-parameters of four 2×2 antenna array MIMO system in orthogonal arrangement.

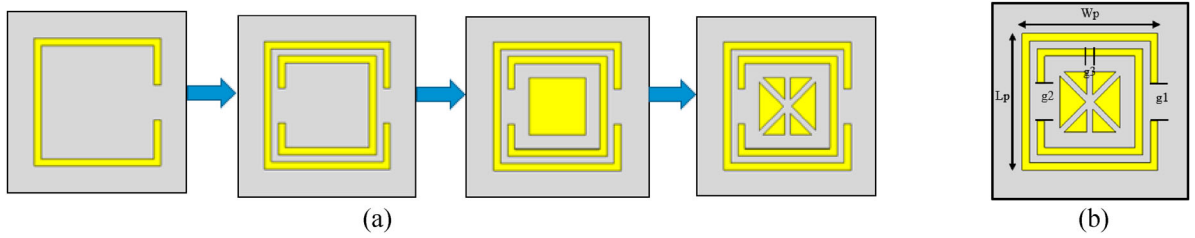


Figure 9. (a) Evolution of the metasurface unit-cell, and (b) proposed metasurface unit-cell.

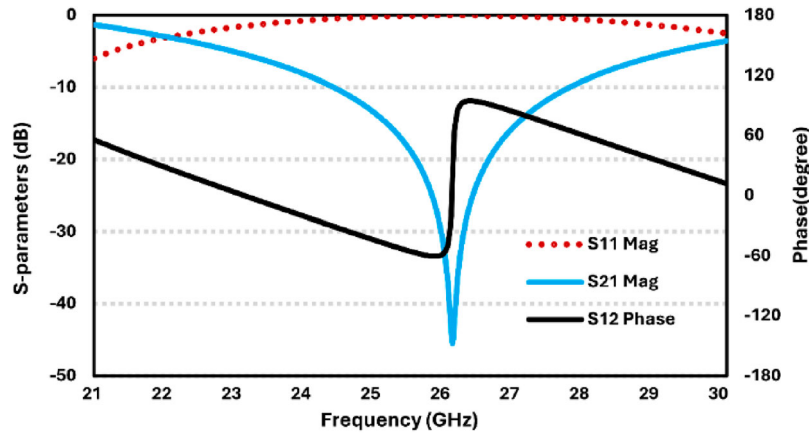
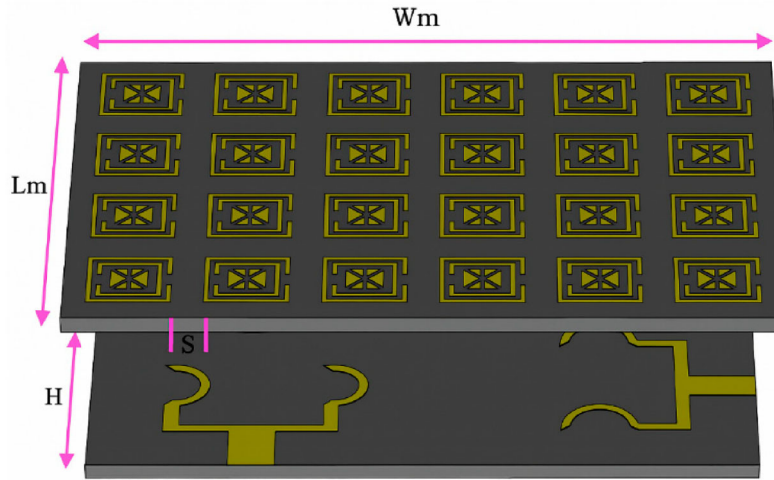
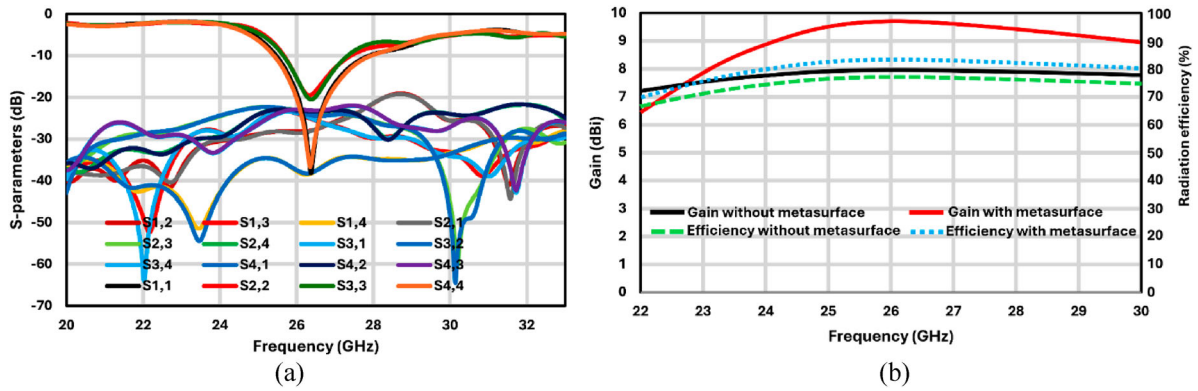


Figure 10. S-parameters (magnitude and phase) of the proposed metasurface unit-cell.

that the angle of refraction of the electromagnetic wave is in the opposite direction compared to conventional materials. This phenomenon is a key characteristic of metasurface. The phase response was enhanced by first adding a square patch in the middle of the unit cell and creating diagonal and a vertical slot through the patch. The dimensions are given in Table 3. Figure 10 shows the magnitude and phase of the S-parameter response using CST Studio Suite, which is a 3D electromagnetic solver based on method of moments technique, by Dassault Systeme. It is evident that the phase change is significant around 26 GHz.

Table 3. Dimensions of the metasurface unit cell.

| Parameter | Values (mm) |
|-----------|-------------|
| Lp | 4.5 |
| Wp | 4.5 |
| g1 | 1.3 |
| g2 | 1.27 |
| g3 | 0.18 |

**Figure 11.** Orthogonal 2×2 radiating element MIMO antenna array with 5×6 metasurface. The gap between unit cells is 1.6 mm, $W_m = 40$ mm, and $L_m = 40$ mm.**Figure 12.** (a) S-parameters of orthogonal 2×2 MIMO antenna array with metasurface, and (b) Gain and radiation efficiency with and without metasurface.

3. MIMO antenna array with metasurface

The metasurface unit cells were arranged in a 5×6 matrix to create a metasurface which is located above the 2×2 antenna array, as illustrated in Figure 11. The space between the array and the metasurface is 10 mm (equivalent to $0.86\lambda_0$ at 26 GHz). The spacing between the unit cells is 1.6 mm ($0.14\lambda_0$ at 26 GHz). Figure 12(a) shows the reflection coefficient response of this arrangement. The reflection coefficient is better than -20 dB at 26.3 GHz, and the inter-element isolation or mutual coupling is higher than 19 dB. Figure 12(b) shows that with the metasurface the gain is improved by 1.5 dB between 25 GHz to 27.5 GHz. This is because the metasurface suppresses cross-polarization, thereby directing more of the radiated energy into the desired co-polarization.

Beyond suppressing cross-polarization, the metasurface enhances gain by acting as a spatial phase-correcting surface. The periodic 5×6 array of rectangular split-ring resonators (RSRs) introduces phase shifts

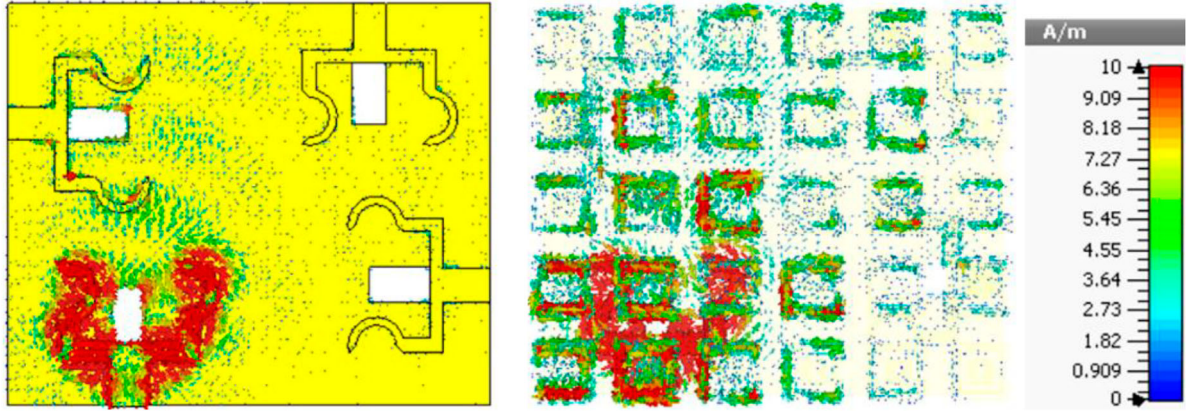


Figure 13. Surface current density distribution over the 2×2 element MIMO antenna and metasurface at 26 GHz.

across the aperture that result in constructive interference along the main radiation direction. This focusing effect increases the array's directivity without altering the feed structure or increasing power consumption. The resonant properties of the RSRs are tailored to operate near 26 GHz, enabling strong electromagnetic coupling with the underlying antenna elements and shaping the outgoing wavefront for improved radiation efficiency.

The difference in S_{11} and S_{33} responses is attributed to the difference in the coupling between antenna elements in a MIMO system. The third element (S_{33}) might experience a different mutual coupling effect compared to the first element (S_{11}), simply due to how these elements interact with their respective neighboring antennas. The orthogonal arrangement of the elements also contributes to this, as mutual coupling is affected by the relative polarization of nearby elements, and these effects might not be symmetrical for all the elements in the array. Moreover, the presence of the metasurface above the antenna array introduces an additional layer of complexity. Ideally, the metasurface enhances gain and directivity, but any misalignment or positioning discrepancy of the metasurface can lead to different responses for each antenna element.

The high isolation in the proposed MIMO antenna system is achieved through a combination of strategic design elements and careful integration of the metasurface, without requiring explicit isolating components. The radiating elements are arranged in an orthogonal configuration, which naturally minimizes coupling since their electric fields are polarized at 90 degrees to each other, reducing mutual interactions. Additionally, a metasurface composed of a 5×6 matrix of split-ring resonators is placed above the antenna array to effectively confine electromagnetic energy to the excited element. This metasurface functions as a spatial filter, suppressing cross-polarization and directing more radiated energy into the desired direction, which reduces unwanted coupling. The elements are spaced approximately $1.5\lambda_0$ apart, further ensuring minimal near-field interaction. A Defected Ground Structure (DGS), featuring rectangular slots under each radiating element, modifies the surface current paths, interrupting surface wave propagation that might otherwise contribute to higher coupling.

Figure 13 displays the surface current distribution across the MIMO antenna array and metasurface at a frequency of 26 GHz when a single antenna element is excited. In the visualization, regions with high current density are highlighted in red. Notably, the current density distribution clearly indicates minimal interaction between neighboring antennas. Furthermore, the distribution of current density over the metasurface is concentrated around the specific port that is excited. This observation suggests that the metasurface effectively confines the current to the excited port, minimizing unwanted interactions between elements in the array.

4. Experimental results

The proposed antenna array and metasurface was fabricated on Rogers RT/duroid 5880. Figure 14 shows the photograph of the array and the metasurface. The metasurface placed above the antenna is supported by low-loss dielectric spacers. The spacers are made from materials, e.g. Polytetrafluoroethylene (PTFE) with a loss tangent of ~ 0.0002 – 0.0004 , with minimal impact on the electromagnetic performance, meaning that they introduce minimal losses or distortions. The exact positioning of the metasurface is critical for ensuring

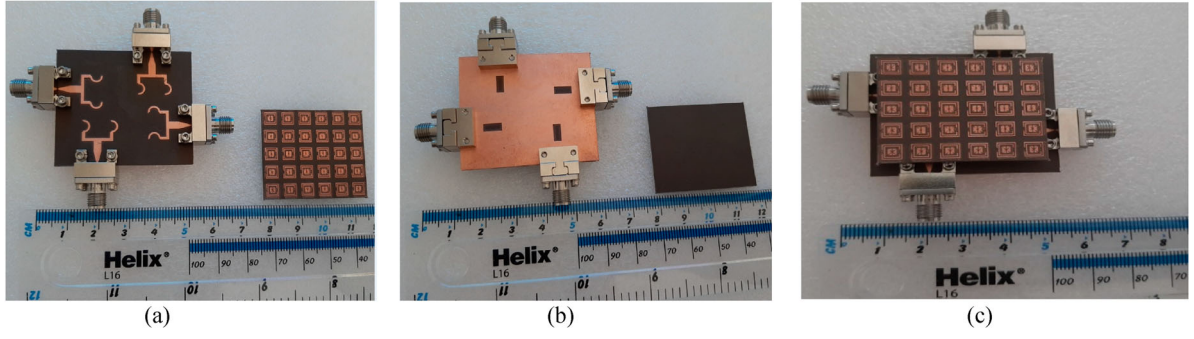


Figure 14. Fabricated prototype of orthogonal 2×2 radiating elements and the metasurface, (a) Front view of top and middle layers, (b) Back view, and (c) Integrated array and metasurface MIMO antenna.

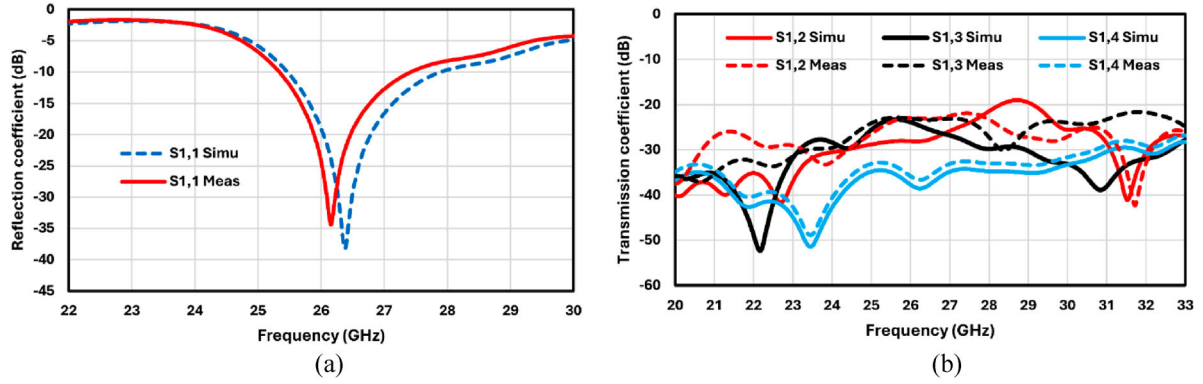


Figure 15. Simulated and measured responses of the integrated array and metasurface MIMO antenna, (a) Reflection coefficient responses, and (b) Transmission coefficient responses.

optimal performance. Any misalignment or deviation from the intended position can have significant impact on the gain and diversity, increased cross-polarization and reduced radiation efficiency.

4.1. S-Parameter response of the proposed MIMO system

The MIMO systems reflection and transmission coefficients, shown in Figure 15, were measured using a Vector Network Analyzer (VNA). The measured S_{11} has a minimum of -34.7 dB at 26.15 GHz, and the simulated reflection coefficient has a minimum value of -38 dB at 26.4 GHz. There is close agreement between the simulated and measured reflection coefficient response. The impedance bandwidth simulated is 2.5 GHz for $S_{11} \leq -10$ dB and the measured bandwidth is 2.2 GHz. The above results are consistent for other MIMO antenna array ports. The measured isolation between the ports is better than 22 dB. The small discrepancies between the simulated and measured results are due to fabrication tolerances and inaccuracies in the simulation models.

The gain of the metasurface integrated antenna array was measured using standard procedure. The measured gain, shown in Figure 16, between 24.6 and 28.7 GHz is above 9 dBi with a peak of 9.4 dBi at 26 GHz.

4.2. Envelope correlation coefficient

The Envelope Correlation Coefficient (ECC) provides insight into the degree of coupling within the MIMO antenna system. In practice, it is generally recommended to maintain an ECC value below 0.5 to effectively minimize undesirable coupling effects. The value of ECC in Figure 17 was calculated using the relation in [21,32]

$$ECC = \frac{|\iint 4\pi (M_i)(\theta, \phi) \times (M_j(\theta, \phi)) d\Omega|^2}{\iint 4\pi |(M_i(\theta, \phi))|^2 d\Omega \iint 4\pi |(M_j(\theta, \phi))|^2 d\Omega} \quad (2)$$

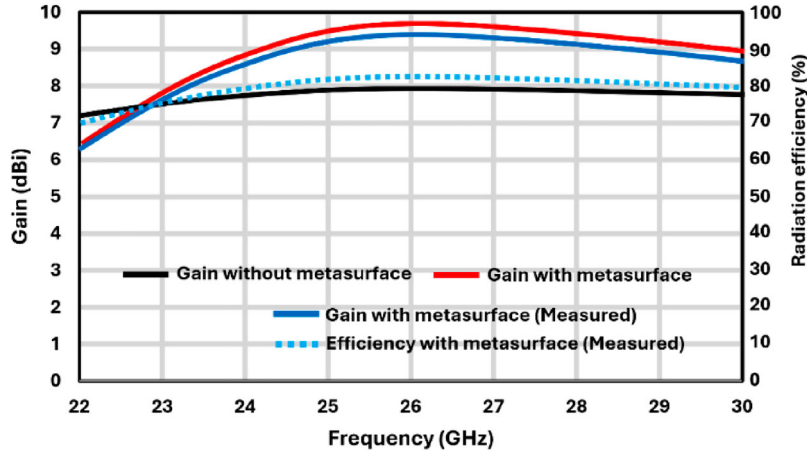


Figure 16. MIMO antenna array gain response with and without the metasurface.

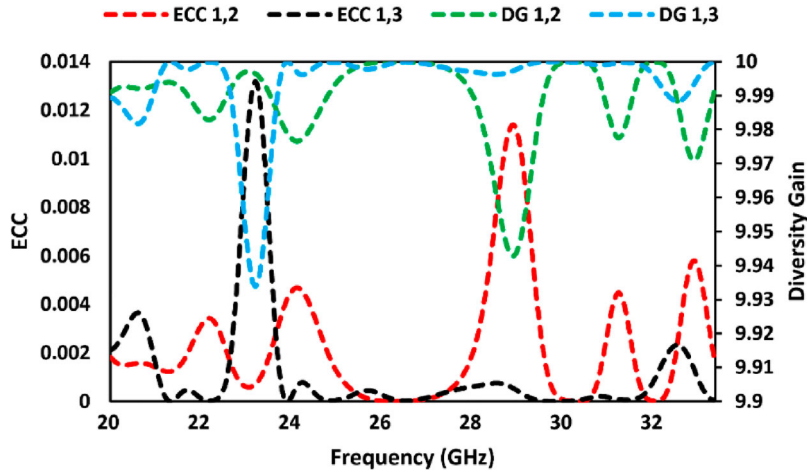


Figure 17. ECC and DG gain performance of the proposed metasurface based MIMO antenna array.

Where $M_i(\theta, \phi)$ and $M_j(\theta, \phi)$ represent the radiation patterns when antennas i and j are excited, respectively; and the term Ω denotes the solid angle.

Specifically, the ECC was computed from the far-field radiation patterns simulated in CST Studio Suite, using the standard integral-based formula that accounts for spatial correlation across all angular directions. This method provides a more accurate and physically meaningful estimate of ECC compared to S-parameter-based approximations, particularly in systems with high isolation and orthogonal polarization. The simulated ECC values remain below 0.0005 across the 25–27 GHz band. In practical terms, ECC values below 0.5 are generally acceptable for MIMO systems, while values below 0.01 are ideal for high-performance 5G applications. The exceptionally low ECC of the proposed antenna array thus confirms its effectiveness in supporting low-correlation, high-diversity MIMO performance.

The proposed MIMO system has an ECC of less than 0.001 inside the desired operating band 25 GHz to 27 GHz. This confirms low coupling among radiating elements.

4.3. Diversity gain

Diversity gain (DG) is one of the basic MIMO parameters which describes the losses during transmission of power when diversity schemes are performed in MIMO system. The diversity gain, shown in Figure 17 was calculated from ECC data using equation (2). DG is over the frequency range of interest is 10 dB.

$$DG = 10 \times \sqrt{1 - ECC} \quad (3)$$

4.4. Channel capacity loss

Channel Capacity Loss (CCL) is an important metric used to assess the performance of MIMO antenna systems. It provides insight into the system's efficiency in terms of data throughput, which directly relates to its effectiveness in real-world applications. The lower the CCL, the more efficient the system is in maintaining high data rates with minimal signal degradation. The CCL is calculated by using the following expression:

$$CCL = -\log_2 \det(\Psi^R) \quad (4)$$

In this expression, Ψ^R represents the correlation matrix of the receiving antenna elements. The correlation matrix helps quantify the interaction between multiple antenna elements, and thus, it measures how effectively each antenna contributes to the overall MIMO performance. A lower correlation indicates better utilization of spatial diversity, which directly impacts channel capacity. The correlation matrix Ψ^R is defined as follows:

$$\Psi^R = \begin{bmatrix} \Psi_{ii} & \Psi_{ij} \\ \Psi_{ji} & \Psi_{jj} \end{bmatrix} \quad (5)$$

In the above matrix, the diagonal elements (Ψ_{ii} and Ψ_{jj}) and the off-diagonal elements (Ψ_{ji} and Ψ_{ij}) describe different relationships between the antenna elements. Specifically:

- Ψ_{ii} and Ψ_{jj} represent the amount of power that is not lost to coupling or correlation between the antenna elements.
- Ψ_{ji} and Ψ_{ij} represent the mutual coupling or interaction between different antenna elements.

These elements are calculated as follows:

$$\Psi_{ii} = 1 - (|S_{ii}|^2 + |S_{ij}|^2) \quad (6)$$

$$\Psi_{ij} = -(S_{ii}^* S_{ij} + S_{ji}^* S_{jj}) \quad (7)$$

$$\Psi_{ji} = -(S_{jj}^* S_{ji} + S_{ij}^* S_{ii}) \quad (8)$$

$$\Psi_{jj} = 1 - (|S_{jj}|^2 + |S_{ji}|^2) \quad (9)$$

Figure 18 shows the performance of the proposed MIMO antenna system in terms of the CCL. It is shown that the CCL value for the entire frequency band of interest is consistently below 0.4 bits/s/Hz. This is a key result, as it satisfies the industry requirement for efficient MIMO operation, which typically demands a CCL value below 0.4 bits/s/Hz to ensure optimal throughput.

4.5. Radiation patterns

The radiating elements in the four-port MIMO system are positioned perpendicular to each other to achieve pattern diversity, which is useful for mitigating the multipath fading experienced in wireless communication systems. The radiation patterns at the two principal planes, namely the E-plane and H-plane at 26 GHz, are shown in Figure 19. The MIMO antenna array's radiation pattern is directional, making it suitable for efficient propagation in atmospheric conditions.

5. Comparison with previous works

In Table 4, the proposed 2×2 element metasurface MIMO antenna array is compared with various representative mmWave and sub-mmWave MIMO antenna arrays found in the literature [33–39]. Most of the arrays listed in the table utilize the widely adopted technique of DGS, which is effective for controlling unwanted radiation patterns and enhancing antenna performance. However, a few of the compared designs, such as those in Refs. [37] and [38], leverage Dielectric Resonator Antennas (DRA), which offer unique advantages such as higher efficiency and better handling of higher frequencies.

When comparing the performance of these antenna arrays, the proposed metasurface-based MIMO antenna array shows competitive results in several key parameters such as size, Envelope Correlation Coefficient (ECC), and inter-element isolation. The size of the proposed array, with dimensions of $36 \times 36 \times 0.8$ mm,

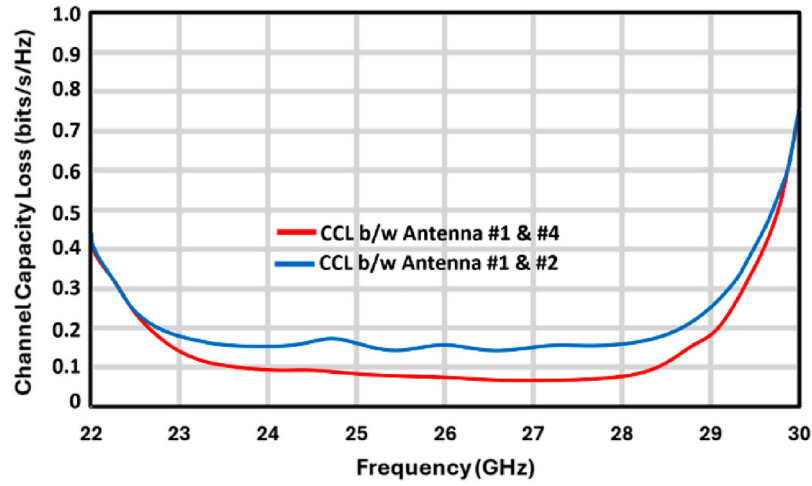


Figure 18. Channel capacity loss (CCL) of the proposed 2×2 element metasurface MIMO antenna array.

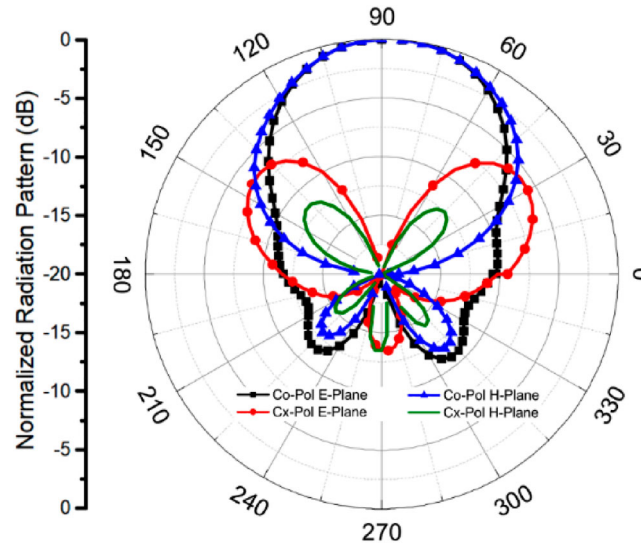


Figure 19. Measured radiation in the E- and H-planes of the 2×2 element metasurface MIMO antenna array at 26 GHz.

Table 4. Comparing the proposed MIMO antenna array with the representative state of the art.

| Ref. | Freq. (GHz) | No. of Ports | Dimensions (mm) | Min. Isolation (dB) | Peak Gain (dBi) | ECC | Techniques |
|-----------|-------------|--------------|-----------------------------|---------------------|-----------------|--------|-------------|
| [33] | 27 | 4 | $30 \times 30 \times 1.575$ | 30 | 7.1 | 0.0005 | DGS |
| [34] | 28 | 4 | $30 \times 35 \times 0.76$ | 17 | 8.3 | <0.01 | DGS |
| [35] | 28 | 2 | $15 \times 25 \times 0.203$ | 30 | 5.8 | <0.005 | DGS |
| [36] | 28 | 4 | $30 \times 30 \times 0.787$ | 29 | 6.1 | <0.16 | DGS |
| [37] | 28 | 4 | $20 \times 40 \times 1.6$ | 29.34 | 7 | <0.01 | DRA |
| [38] | 27 | 4 | $30 \times 28 \times 0.508$ | 24 | 6.22 | <0.05 | DGS |
| [39] | 28 | 2 | $18 \times 38 \times 0.8$ | 64 | 8.75 | <0.005 | DGS |
| This work | 26 | 4 | $36 \times 36 \times 0.8$ | 22 | 9.4 | <0.005 | Metasurface |

is comparable to the arrays found in [33,34], and [36], where the array sizes range from 30×30 mm to 30×40 mm. Despite the relatively compact size, the proposed antenna array exhibits a remarkable performance in terms of inter-element isolation and peak gain.

In terms of isolation, a critical performance metric for MIMO systems, the proposed antenna array achieves a minimum isolation of 22 dB, which is higher than the isolation levels of many of the arrays in the literature. For example, arrays in [33,34,36,38] report minimum isolation values ranging from 17 dB to 30 dB, with some achieving isolation as high as 64 dB [39]. The enhanced isolation in the proposed metasurface design

helps minimize signal interference between antenna elements, leading to better overall system performance, especially in multi-path environments.

Furthermore, the peak gain of the proposed antenna array reaches 9.4 dBi, which is significantly higher than many of the other arrays. For instance, arrays in [33], [35], and [38] report peak gains in the range of 5.8 dBi to 8.3 dBi. The higher peak gain of the proposed array is advantageous in increasing the effective communication range and improving the signal strength, which is crucial in mmWave and sub-mmWave MIMO systems where signal attenuation is a major concern.

Additionally, the ECC of the proposed antenna array is < 0.005 , which is comparable to the very low ECC values reported in the cited works. This low ECC is an important factor in ensuring that the antenna elements are effectively decoupled, which leads to enhanced diversity and improved MIMO performance.

6. Conclusion

This study demonstrates the feasibility of integrating a metasurface cover with a millimeter-wave MIMO antenna array operating at 26 GHz. The 2×2 antenna array is designed with the radiation elements arranged in an orthogonal configuration, which helps minimize mutual coupling and electromagnetic interference between the elements. As a result, the antenna's radiation performance is significantly improved. The array achieves a gain of over 9 dBi across the frequency range of 24.6 GHz to 28.7 GHz, with a peak gain of 9.4 dBi at 26 GHz. The introduction of the metasurface above the array plays a key role in this performance boost by precisely controlling the phase and amplitude of the incident wave through its unique structure. Additionally, the proposed MIMO system exhibits an exceptionally low ECC of less than 0.001 within its operating band of 25 GHz to 27 GHz. This indicates minimal coupling between the antenna elements and highlights the effectiveness of the metasurface integration in improving overall antenna performance.

Acknowledgments

Co-funded by the European Union. Views and opinions expressed are however those of the author(s) only and do not necessarily reflect those of the European Union or the European Research Executive Agency. Neither the European Union nor the granting authority can be held responsible for them. Besides that, this publication has emanated from research jointly funded by Taighde Éireann – Research Ireland under Grant number 13/RC/2094_2, the European Union's Marie Skłodowska-Curie Actions under grant number 101126578 and was supported in part by University of Galway. In addition, the authors appreciate the Princess Nourah bint Abdulrahman University Researchers Supporting Project number (PNURSP2025R828), Princess Nourah bint Abdulrahman University, Riyadh, Saudi Arabia.

Author contributions

CRedit: **Mohammad Alibakhshikenari**: Conceptualization, Data curation, Formal analysis, Funding acquisition, Investigation, Methodology, Project administration, Resources, Software, Validation, Visualization, Writing – original draft, Writing – review & editing; **Iftikhar ud Din**: Data curation, Formal analysis, Methodology, Resources, Software, Validation, Writing – original draft, Writing – review & editing; **Esraa Mousa Ali**: Methodology, Resources, Validation, Writing – review & editing; **Noof Abd Elmunim**: Funding acquisition, Validation, Visualization, Writing – review & editing; **Bal S. Virdee**: Conceptualization, Investigation, Methodology, Software, Validation, Writing – review & editing; **Dion Mariyanayagam**: Data curation, Investigation, Software, Validation, Writing – review & editing; **Sadiq Ullah**: Data curation, Formal analysis, Visualization, Writing – review & editing; **Nisar Ahmad Abbasi**: Data curation, Formal analysis, Resources, Validation, Writing – review & editing; **Nasr Rashid**: Conceptualization, Formal analysis, Validation, Visualization, Writing – review & editing; **Chan Hwang See**: Conceptualization, Data curation, Formal analysis, Resources, Validation, Writing – review & editing; **Takfarinas Saber**: Conceptualization, Formal analysis, Investigation, Project administration, Resources, Supervision, Validation, Writing – review & editing; **Francisco Falcone**: Funding acquisition, Methodology, Project administration, Resources, Validation, Writing – review & editing; **Ernesto Limiti**: Conceptualization, Methodology, Project administration, Resources, Supervision, Validation, Visualization, Writing – review & editing

Disclosure statement

No potential conflict of interest was reported by the authors.

References

- [1] Tantawy ZH, El Mashade MB, Emran AA, et al. On the performance of FSO communication system with WDM

- and MIMO structure under different turbulent atmospheric conditions. *J Opt Commun*. 2024;45(s1):s2133–s2149. doi:10.1515/joc-2023-0099
- [2] Qasem N. Measurement and simulation for improving indoor wireless communication system performance at 2.4 GHz by modifying the environment. *IEEE Access*. 2024;12:96660–96671. doi:10.1109/ACCESS.2024.3426490
 - [3] Iskandarani MZ. Investigation of energy consumption in WSNs within enclosed spaces using beamforming and LMS (BF-LMS). *IEEE Access*. 2024;12:63932–63941.
 - [4] Elsharief M, Emran AA, Hassan H, et al. SLES: scheduling-based low energy synchronization for industrial internet of things. *IEEE Sensors J*. 2022;22(16):16652–16661.
 - [5] Etman AM, Abdalzaher MS, Emran AA, et al. A survey on machine learning techniques in smart grids based on wireless sensor networks. *IEEE Access*. 2025;13:2604–2627.
 - [6] Qualcomm Technologies Inc. Spectrum for 4G and 5G. [cited 2019 Jan 5]. Available from: <https://www.qualcomm.com/news/media-center>.
 - [7] Wang CX, et al. Cellular architecture and key technologies for 5G wireless communication networks. *IEEE Commun Mag* 2014;52(2):122–130.
 - [8] Hussain N, Jeong M-J, Abbas A, et al. A metasurface-based low-profile wideband circularly polarized patch antenna for 5G millimeter-wave systems. *IEEE Access*. 2020;8:22127–22135.
 - [9] Abdullah M, Kiani SH, Iqbal A. Eight element multiple-input multiple-output (MIMO) antenna for 5G mobile applications. *IEEE Access*. 2019;7:134488–134495.
 - [10] Wang F, Duan Z, Wang X, et al. High isolation millimeter-wave wideband MIMO antenna for 5G communication. *Int J Antennas Propag*. 2019;2019:4283010. doi:10.1155/2019/4283010
 - [11] Kiani SH, Altaf A, Abdullah M, et al. Eight element side edged framed MIMO antenna array for future 5G smart phones. *Micromachines (Basel)*. 2020;11:956. doi:10.3390/mi11110956
 - [12] Guo J, Cui L, Li C, et al. Side-edge frame printed eight-port dual-band antenna array for 5G smartphone applications. *IEEE Trans Antennas Propag*. 2018;66:7412–7417. doi:10.1109/TAP.2018.2872130
 - [13] Zhu Q, Ng KB, Chan CH, et al. Substrate-integrated-waveguide-fed array antenna covering 57–71 GHz band for 5G applications. *IEEE Trans Antennas Propag*. 2017;65:6298–6306. doi:10.1109/TAP.2017.2723080
 - [14] Shayeia I, Abd Rahman T, Hadri Azmi M, et al. Real measurement study for rain rate and rain attenuation conducted over 26 GHz microwave 5 g link system in Malaysia. *IEEE Access*. 2018;6:19044–19064. doi:10.1109/ACCESS.2018.2810855
 - [15] Malik BT, et al. Antenna gain enhancement by using low-infill 3D-printed dielectric lens antennas. *IEEE Access*. 2019;7:102467–102476. doi:10.1109/ACCESS.2019.2931772
 - [16] Hussain N, Park I. Performance of multiple feed metasurface antennas with different numbers of patch cells and different substrate thicknesses. *Appl Comput Electromagn J*. 2018;33(1):49–55.
 - [17] Asaadi M, Affi I, Sebak A-R. High gain and wideband high dense dielectric patch antenna using FSS superstrate for millimeter-wave applications. *IEEE Access*. 2018;6:38243–38250.
 - [18] Rahman M, Nagshvarian Jahromi M, Mirjavadi SS, et al. Compact UWB band-notched antenna with integrated Bluetooth for personal wireless communication and UWB applications. *Electronics (Basel)*. 2019;8:158.
 - [19] Ojaroudi Parchin N, Jahanbakhsh Basherlou H, Alibakhshikenari M, et al. Mobile-phone antenna array with diamond-ring slot elements for 5G massive MIMO systems. *Electronics (Basel)*. 2019;8:521.
 - [20] Kulkarni J, et al. A compact four port ground-coupled CPWG-fed MIMO antenna for wireless applications. *Arab J Sci Eng*. 2022;47:14087–14103.
 - [21] Kulkarni J, et al. A dual-CP quad-port MIMO antenna with reduced mutual coupling for X-band application. *IEEE Antennas Wirel Propag Lett*. 2023;22:2085–2089. doi:10.1109/LAWP.2023.3275530
 - [22] Kulkarni J, et al. Wideband four-port MIMO antenna array with high isolation for future wireless systems. *AEUE - International Journal of Electronics and Communications*. 2021;128:153507. doi:10.1016/j.aeue.2020.153507
 - [23] Le TH, et al. Wide band dual polarized antenna array for 5G mmWave based massive MIMO base station applications. 2022 24th International Microwave and Radar Conference (MIKON), Gdansk, Poland. 2022. p. 1–4. doi:10.23919/MIKON54314.2022.9924917
 - [24] Li A, Singh S, Sievenpiper D. Metasurfaces and their applications. *Nanophotonics*. 2018;7(6):989–1011. doi:10.1515/nanoph-2017-0120
 - [25] Jiang H, Si L-M, Hu W, et al. A symmetrical dual-beam bowtie antenna with gain enhancement using metamaterial for 5G MIMO applications. *IEEE Photon J*. 2019;11(1):1–9.
 - [26] Iqbal A, Basir A, Smida A, et al. Electromagnetic bandgap backed millimeter-wave MIMO antenna for wearable applications. *IEEE Access*. 2019;7:111135–111144. doi:10.1109/ACCESS.2019.2933913
 - [27] Murthy NS. Improved isolation metamaterial inspired mm-wave MIMO dielectric resonator antenna for 5G application. *Prog. Electromagn. Res.C*. 2020;100:247–261. doi:10.2528/PIERC19112603
 - [28] Saad AAR, Mohamed HA. Printed millimeter-wave MIMO based slot antenna arrays for 5G networks. *AEU Int. J. Electron. Commun*. 2019;99:59–69. doi:10.1016/j.aeue.2018.11.029
 - [29] Sharawi MS, Podilchak SK, Hussain MT, et al. Dielectric resonator based MIMO antenna system enabling millimetre wave mobile devices. *IET Microw., Antennas Propag*. 2017;11(2):287–293. doi:10.1049/iet-map.2016.0457
 - [30] Din IU, Ullah S, Naqvi SI, et al. Improvement in the gain of UWB antenna for GPR applications by using frequency-selective surface. *Int J Antennas Propag*. 2022;2022:2002552. doi:10.1155/2022/2002552

- [31] Din IU, Ullah S, Mufti N, et al. Metamaterial-based highly isolated MIMO antenna system for 5G smartphone application. *Int J Commun Syst.* **2023**;36:e5392. doi:[10.1002/dac.5392](https://doi.org/10.1002/dac.5392)
- [32] Saadh AM, Ashwath K, Ramaswamy P, et al. A uniquely shaped MIMO antenna on FR4 material to enhance isolation and bandwidth for wireless applications. *AEU-Int J Electron Commun.* **2020**;123:153316.
- [33] Hussain N, Awan WA, Ali W, et al. Compact wideband patch antenna and its MIMO configuration for 28 GHz applications. *AEU-Int J Electron Commun.* **2021**;132:153612.
- [34] Hussain M, Mousa Ali E, Jarchavi SMR, et al. Design and characterization of compact broadband antenna and its MIMO configuration for 28 GHz 5G applications. *Electronics (Basel).* **2022**;11(4):523. doi:[10.3390/electronics11040523](https://doi.org/10.3390/electronics11040523)
- [35] Khalid M, Iffat Naqvi S, Hussain N, et al. 4-Port MIMO antenna with defected ground structure for 5G millimeter wave applications. *Electronics (Basel).* **2020**;9(1):71. doi:[10.3390/electronics9010071](https://doi.org/10.3390/electronics9010071)
- [36] Zahra H, Awan WA, Ali WAE, et al. A 28 GHz broadband helical inspired end-fire antenna and its MIMO configuration for 5G pattern diversity applications. *Electronics (Basel).* **2021**;10(4):405. doi:[10.3390/electronics10040405](https://doi.org/10.3390/electronics10040405)
- [37] Kamal MM, Yang S, Ren XC, et al. Infinity shell shaped MIMO antenna array for mm-wave 5G applications. *Electronics (Basel).* **2021**;10(2):165. doi:[10.3390/electronics10020165](https://doi.org/10.3390/electronics10020165)
- [38] Murthy N. Improved isolation metamaterial inspired mm-wave MIMO dielectric resonator antenna for 5G application. *Progress in Electromagnetics Research C.* **2020**;100:247–261. doi:[10.2528/PIERC19112603](https://doi.org/10.2528/PIERC19112603)
- [39] Khalid H, Khalid M, Fatima A, et al. MIMO antenna with defected ground structure for mm-wave 5G applications. *13th international conference on mathematics, actuarial science, computer science and statistics (MACS)*, **2019**. p. 1–6.